Detection and Classification of Hyperfine-Shifted ^{1}H, ^{2}H, and ^{15}N Resonances of the Rieske Ferredoxin Component of Toluene 4-Monooxygenase†

Bin Xia,[‡,§,||] Jeremie D. Pikus,[§,⊥] Weidong Xia,[‡] Kevin McClay,[#] Robert J. Steffan,[#] Young Kee Chae,[⊥] William M. Westler,[§] John L. Markley,*[,§] and Brian G. Fox*[,§,⊥]

The Institute for Enzyme Research, Graduate School, University of Wisconsin, Madison, Wisconsin 53705, Department of Biochemistry, College of Agricultural and Life Sciences, University of Wisconsin, Madison, Wisconsin 53706, and Envirogen, Inc., Lawrenceville, New Jersey 08648

Received August 3, 1998; Revised Manuscript Received November 4, 1998

ABSTRACT: T4MOC is a 12.3 kDa soluble Rieske ferredoxin that is obligately required for electron transfer between the oxidoreductase and diiron hydroxylase components of toluene 4-monooxygenase from *Pseudomonas mendocina* KR1. Our preliminary ^{1}H NMR studies of oxidized and reduced T4MOC [Markley, J. L., Xia, B., Chae, Y. K., Cheng, H., Westler, W. M., Pikus, J. D., and Fox, B. G. (1996) in *Protein Structure Function Relationships* (Zaidi, Z., and Smith, D., Eds.) pp 135−146, Plenum Press, London] revealed the presence of hyperfine-shifted ^{1}H resonances whose short relaxation times made it impractical to use nuclear Overhauser effect (NOE) measurements for assignment purposes. We report here the use of selective isotopic labeling to analyze the hyperfine-shifted ^{1}H, ^{2}H, and ^{15}N signals from T4MOC. Selective deuteration led to identification of signals from the four H$^\beta$ atoms of cluster ligands C45 and C64 in the oxidized and reduced forms of T4MOC. In the reduced state, the Curie temperature dependence of the H$^\beta$ protons corresponded to that predicted from the simple vector spin-coupling model for nuclei associated with the localized ferric site. The signal at 25.5 ppm in the ^{1}H spectrum of reduced T4MOC was assigned on the basis of selective ^{2}H labeling to the His H$^{\epsilon 1}$ atom of one of the cluster ligands (H47 or H67). This assignment was corroborated by a one bond ^{1}H−^{13}C correlation (at 25.39 ppm ^{1}H and 136.11 ppm ^{13}C) observed in spectra of [*U*-^{13}C]T4MOC with a ^{1}H−^{13}C coupling constant of ∼192 Hz. The carbon chemical shift and one bond coupling constant are those expected for ^{1}H$^{\epsilon 1}$−^{13}C$^{\epsilon 1}$ in the imidazolium ring of histidine and are inconsistent with values expected for cysteine ^{1}H$^\alpha$−^{13}C$^\alpha$. The His H$^{\epsilon 1}$ proton exhibited weak Curie temperature dependence from 283 to 303 K, contrary to the anti-Curie temperature dependence predicted from the spin coupling model for nuclei associated with the localized ferrous site. A ^{1}H peak at −12.3 ppm was observed in spectra of reduced T4MOC; this signal was found to correspond to a hydrogen (probably in an H-bond to the cluster) that exchanged with solvent with a half-time of about 2 days in the oxidized state but with a much longer (undetectable) half-time in the reduced state. These results with T4MOC call into question certain ^{1}H assignments recently reported on the basis of NOE measurements for the comparable Rieske ferredoxin component of an evolutionarily related alkene monooxygenase from *Xanthobacter* sp. Py2 [Holz, R. C., Small, F. J., and Ensign, S. A, (1997) *Biochemistry* 36, 14690−14696]. Selective ^{15}N labeling was used to identify hyperfine-shifted ^{15}N NMR signals from the backbone nitrogens of all four cluster ligands (C45, H47, C64, and H67), from the N$^{\epsilon 2}$ atoms of the two histidine ligands (H47 and H67), and from nonligand Gln and Ala residues (Q48 and A66) present in the cluster-binding motif of T4MOC in the oxidized and reduced states. The results indicate that the N$^{\delta 1}$ of each of the two ligand histidines of T4MOC are ligated to an iron atom and reveal a pattern of H-bonding to the Rieske [2Fe-2S] center involving four (H47, Q48, A66, and H67 of T4MOC) of the five backbone amide H-bonds expected on the basis of comparison with the crystal structures of other related Rieske proteins; the fifth backbone amide (I50 of T4MOC) failed to exhibit a hyperfine shift. This anomaly may arise from the lack of an associated disulfide in T4MOC, a fundamental structural difference between the three types of Rieske proteins that may be related to functional diversity in this protein family.

Rieske [2Fe-2S] centers are found in the cytochrome oxidase complexes (*1*), in the oxygenase components of enzymes such as the benzene, naphthalene, phthalate, and toluene dioxygenases (*2*), and in small M_r ferredoxins that act as soluble electron carriers for a variety of bacterial oxygenases (*3*). Figure 1 shows the metal-binding motif C−X−H−X_{15-21}−C−X_2−H that has been identified in all Rieske proteins (*2*). Spectroscopic studies have revealed an asymmetric iron−sulfur core with the S$^\gamma$ atom of each of the two cysteine residues coordinated to one iron site and with the N$^{\delta 1}$ atom of each of the two histidine residues coordinated to the other iron site (*4*−*9*). Mössbauer and ENDOR studies have shown that the His-coordinated iron becomes a localized ferrous site upon reduction (*4*−*6*).

10.1021/bi981851a CCC: $18.00
Published on Web 12/22/1998

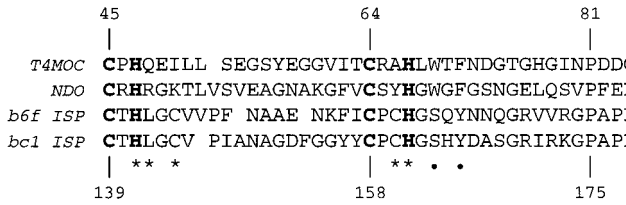

FIGURE 1: Comparison of the amino acid sequences providing the CXH and CXXH iron binding motif in T4MOC, naphthalene dioxygenase (*13*), and the ISP domains of the chloroplastic cytochrome b_6f complex (*12*) and bovine heart mitochondrial bc_1 complex (*10*). Gaps have been inserted into the sequence between the metal binding motifs to align the metal cluster ligands. The numbering of T4MOC is based on nucleotide sequencing, whereas the numbering of the ISP fragment is that used for the bovine complex (*10*). The five residues identified in the ISP structure to provide peptidyl N−H bonds to the cluster are indicated (*); the serine and tyrosine residues identified in the ISP structure to provide H-bonding via their hydroxyl groups are indicated (●). The latter two residues are not conserved in T4MOC.

Crystal structures of the Rieske ISP[1] domains from the bovine mitochondrial bc_1 oxidase (*10, 11*), the chloroplastic cytochrome b_6f oxidase (*12*), and NDO (*13*) confirmed the predicted ligation motif and revealed the existence of an extensive network of H-bonds to the iron center. In the ISP Rieske domains, the H^N of each of the two histidines that ligate the cluster, the H^N of each of the two cysteines involved in the disulfide bridge adjacent to the cluster, and the hydroxyl groups of one serine and one tyrosine donate H-bonds to sulfur atoms of the cluster (an inorganic sulfide atom and a sulfur atom of one cysteine ligand, respectively).

Recently, we reported the overexpression, purification, and spectroscopic characterization of toluene 4-monooxygenase (T4MO) from *Pseudomonas mendocina* KR1 (*14*). This four protein complex consists of an NADH oxidoreductase, a catalytic effector protein (T4MOD), a diiron center-containing hydroxylase, and a small M_r soluble ferredoxin (T4MOC, 12 326 Da) that is obligately required for catalytic activity. Along with sequence information (Figure 1), optical, EPR, and Mössbauer studies have established that T4MOC contains a Rieske [2Fe-2S] center (*14, 15*). Sequence alignments also revealed that Cys residues comparable to those forming the disulfide bond in the ISP domains are not present in either T4MOC or NDO (Figure 1); in T4MOC, the corresponding residues are I50 and A66. Similarly, the serine and tyrosine residues whose side chains have been shown to participate in H-bonding of the ISP domains are not conserved in either T4MOC or NDO. In NDO, W106 occupies the position corresponding to S163 in the ISP domain and covers one side of the Rieske center (*13*). T4MOC also has tryptophan in this position, W69. The degree to which these structural variations contribute to the functional properties of the members of the Rieske protein family has not been established, although correlations between H-bonding and redox properties have recently been proposed for the ISP Rieske protein (*16*).

NMR spectroscopy has proven to be a powerful technique for characterizing various classes of iron sulfur proteins. Although extensive NMR studies of plant-type and vertebrate [2Fe-2S] ferredoxins are available, only a limited level of detail has been accumulated on the Rieske ferredoxins. The goal of the present study has been to obtain chemical information about the iron−sulfur active site of T4MOC, and to compare these data with other Rieske proteins and [2Fe-2S] ferredoxins. We originally reported paramagnetically shifted ^{1}H NMR signals from T4MOC (*17*), and a more recent study by Holz and co-workers showed that the comparable Rieske ferredoxin component of the alkene epoxidase from *Xanthobacter* sp. Py2 has a similar pattern of paramagnetically shifted ^{1}H NMR signals (*18*). Holz and co-workers assigned these resonances by residue and atom type on the basis of comparison to previous NMR studies of [2Fe-2S] ferredoxins, one-dimensional NOE measurements, and analysis of the temperature dependence of chemical shifts (*18*). Here, we report the use of selective isotope labeling to determine the origin of the paramagnetically shifted ^{1}H, ^{2}H, and ^{15}N resonances of T4MOC. The paramagnetic ^{1}H NMR signals from T4MOC differ in fundamental ways from those of the plant-type and vertebrate ferredoxins, and unambiguous assignments of these signals to residue and atom type in T4MOC call into question certain ^{1}H NMR assignments made for the *Xanthobacter* Rieske center. Furthermore, although the pattern of H-bonding to the iron−sulfur cluster revealed by the ^{15}N-labeling experiments is overall consistent with that observed in the crystal structures of the bc_1 and b_6f ISP domains and NDO, the present results reveal a specific difference in H-bonding to the iron−sulfur cluster of T4MOC associated with the absence of a disulfide bridge in T4MOC. We hypothesize that this difference may ultimately play an important role in the electron-transfer functions of these proteins.

MATERIALS AND METHODS

Construction of Expression Vector pJP01. All materials used to produce vector pJP01 were of the highest purity available and were used without further purification. Vent DNA polymerase, DNA ligase, and restriction endonucleases *Nde*I and *Bam*HI were from New England Biolabs (Beverley, MA). The complete T4MO gene cluster *(tmoABCDEF)* contained in the expression vector pRS184f was used as the

† This work was supported by grants from the Petroleum Research Foundation (ACS-PRF 28405-G4 and ACS-PRF 32955-AC4 to B.G.F.), the NSF (MCB-9733734 to B.G.F.), the NIH (GM-35976 to J.L.M.), and the NSF Small Business Innovation Research Program Grant (DMI-9460076 to R.J.S.). NMR studies were carried out in the National Magnetic Resonance Facility at Madison, which is supported by grants to J.L.M. from the NIH Biomedical Research Technology Program (RR02301), the NSF Biological Instrumentation Program (DMB-8415048), the NSF Shared Instrumentation Program (RR02781), the U.S. Department of Agriculture, and the University of Wisconsin. B.G.F. is a Searle Scholar of the Chicago Community Trust (1994−1997) and a Shaw Scientist of the Milwaukee Foundation (1994−1999).

* To whom correspondence should be addressed. E-mail: fox@enzyme.wisc.edu. Phone: (608) 262-9708. E-mail: markley@nmrfam.wisc.edu. Phone: (608) 263-9349.

‡ Graduate Program in Biophysics, University of Wisconsin−Madison.

§ Department of Biochemistry, University of Wisconsin−Madison.

|| Present address: Department of Molecular Biology, MB-2, The Scripps Research Institute, 10550 N. Torrey Pines Road, La Jolla, CA 92037.

⊥ Institute for Enzyme Research.

Envirogen.

[1] Abbreviations: bc_1, bovine mitochondrial bc_1 ubiquinone cytochrome *c* oxidoreductase; b_6f, chloroplastic b_6f complex; HMQC, heteronuclear multiple-quantum correlation spectroscopy; ISP, iron−sulfur protein domain of the bc_1 or b_6f complexes; NOE, nuclear Overhauser effect; NDO, naphthalene dioxygenase; NMR, nuclear magnetic resonance; T4MOC, 12.3 kDa soluble Rieske-like ferredoxin from *Pseudomonas mendocina* KR1 produced heterologously in *Escherichia coli*.

template for amplification by a polymerase chain reaction (*14*). To facilitate the isotopic labeling of T4MOC for the present studies and to provide for simultaneous isotopic enrichment of T4MOD (11.6 kDa) for related NMR studies, the genes encoding both of these proteins were targeted for coexpression. Primers tmoC5′ (gtagcgCaTatgagctttgaa) and tmoD3′ (tcttggatCcaaagctcatggtgccc) (Integrated DNA Technologies, Coralville, IA) were used to amplify a 751 bp fragment containing these two genes. Primer tmoC5′ contained two base pair mismatches that introduced an *Nde*I restriction site at the *tmoC* ATG start codon (mutations indicated by uppercase in the primer sequence), whereas primer tmoD3′ introduced a *Bam*HI restriction site 8 base pairs downstream of the *tmoD* stop codon. The polymerase chain reaction was performed using the buffer conditions recommended by the supplier. The cycle of melt for 1 min at 94 °C, anneal for 30 s at 50 °C, and extend for 50 s at 72 °C was repeated 25 times. The amplified product was extracted with phenol:chloroform (1:1, v/v) to remove protein, digested with *Nde*I and *Bam*HI, and then analyzed by agarose electrophoresis using a 0.8% agarose gel. The correct band was extracted by electroelution into filter paper, and was then ligated into the similarly digested plasmid pT7Blue (Novagen, Madison WI). The ligated plasmid was transformed into calcium-chloride-competent *E. coli* NovaBlue cells (Novagen) and plated onto Luria-Bertani agar plates containing ampicillin (100 μg/mL) that were top-spread with isopropyl-β-D-thiogalactopyranoside (IPTG) and 5-bromo, 4-chloroindoyl-β-D-galactopyranoside. Plasmid DNA was prepared from 20 of the resulting white colonies using the Wizard Mini-Prep kit (Promega, Madison, WI) and analyzed by restriction digestion mapping to verify the presence of a 751 bp fragment with the correct restriction pattern. The *tmoCD* gene fragment was cut from the agarose gel, extracted as above, and ligated into the similarly digested plasmid pET3a (Novagen). The ligated plasmid was transformed into calcium chloride-competent *E. coli* BL21(DE3) cells (Novagen), and the transformation was selected on Luria-Bertani agar plates containing ampicillin (100 μg/mL). Plasmid DNA was prepared from 20 colonies that exhibited antibiotic resistance and analyzed by restriction digestion mapping. Eight of the colonies contained the correct insert. One of these colonies was picked for propagation, and the plasmid contained in this expression host was designated pJP01. The nucleotide sequences of the *tmoC* and *tmoD* genes were determined at the University of Wisconsin Biotechnology Center by cycle sequencing using AmpliTaq DNA polymerase, FS (Perkin-Elmer, Culver City, CA) and dye-labeled terminators. The determined sequence was found to exactly match that previously published (*19*). The expression host was maintained on Luria-Bertani agar plates containing ampicillin (400 μg/mL), and frozen cell stocks were prepared as previously described (*20*).

Expression of Natural Abundance T4MOC. A frozen cell stock (1 mL) was used to inoculate 500 mL of Luria-Bertani medium containing ampicillin (400 μg/mL) in a 2 L Erlenmeyer flask. This shaken flask culture was grown to an optical density at 600 nm (OD_{600}) of ∼1, and the entire culture was then used to inoculate a benchtop fermenter (Virtis, Vineland, NJ) containing 14 L of Luria-Bertani medium. The culture was grown at pH 7 and 37 °C to an OD_{600} of ∼3−4 and was then induced by the sterile addition of IPTG to a final concentration of 0.1 mM. After 4 h, the cells were harvested by tangential flow filtration and pelleted by centrifugation at 15000*g* for 30 min. The resulting cell pellet was frozen and stored at −80 °C until needed.

Expression of [U-^{15}N]- and [U-^{13}C]-T4MOC. For ^{15}N uniform labeling, the expression host was grown on minimal medium (*21*) containing 0.6% (w/v) glucose as the carbon source and 1.0 g/L of $^{15}NH_4Cl$ as the sole nitrogen source (Cambridge Isotope Labs, Andover, MA, ≥98% isotopic enrichment). For ^{13}C uniform labeling, the expression host was grown on minimal medium (*21*) containing [*U*-^{13}C]-D-glucose (3.0 g/L, minimum 99 atom % ^{13}C, Isotech, Miamisburg, OH) as the carbon source and 1.0 g/L of NH_4Cl as the sole nitrogen source (Cambridge Isotope Labs, Andover, MA, ≥98% isotopic enrichment). Glucose and NH_4Cl were added by filter sterilization after the heat-sterilized medium had cooled. A 50 mL shaken flask culture containing ampicillin (400 μg/mL) was inoculated with 25 μL of cell stock and was grown to an OD_{600} of ∼0.1. This entire culture was then used to inoculate a 500 mL shaken flask culture. The 500 mL culture was grown to $OD_{600} \approx 1$, and the entire culture was then used to inoculate a 4 L BioFlo 3000 benchtop fermenter (New Brunswick Scientific, New Brunswick, NJ). The fermenter culture was grown at pH 7 and 37 °C to an OD_{600} of ∼0.8, with dissolved O_2 held constant at 20% of saturation. The culture was then induced by the addition of IPTG to a final concentration of 0.1 mM. After 3−4 h, the cells were harvested and stored as described above.

Selective Labeling of Cys and His. The atom-naming conventions used here are from the recently proposed standardization of terminology for protein NMR studies (*22*). Selectively labeled amino acids [98% $^2H^{\alpha}$]Cys, [95−99% $^2H^{\beta2,\beta3}$]Cys, [≥98% ^{15}N]Cys, [≥98% ^{15}N]His, [≥98% $^{15}N^{\delta1}$]-His, [≥98% ^{15}N]Ala, [≥98% ^{15}N]Ile, and [≥98% ^{15}N]Gln were obtained from Cambridge Isotope Laboratories; [≥98% $^{15}N^{\delta1,\epsilon2}$]D,L-His was obtained from the Los Alamos Stable Isotope Resource. [≥90% $^2H^{\epsilon1}$]His was prepared by heating [NA]His in D_2O buffered at pH 8 for 8 h at 96 °C (*23*); the percentage of isotopic substitution was confirmed by ^{1}H NMR.

For selective labeling of cysteine, plasmid pJP01 was transformed into the cysteine auxotroph *E. coli* JM15 *(cysE50, tfr-8)* (*24*); for selective labeling of histidine, plasmid pJP01 was transformed into the histidine auxotroph *E. coli* AW608Thr$^+$T7/pLysS (*25*).

The minimal medium used for preparation of T4MOC selectively labeled in either cysteine or histidine was as described for the expression of [*U*-^{15}N]T4MOC except for the substitution of 1 g/L of NH_4Cl and supplementation with the following L-amino acids (g/L, added before heat sterilization): alanine, 0.50; arginine, 0.40; aspartate, 0.40; asparagine, 0.40; glutamine, 0.65; glutamate, 0.65; glycine, 0.55; isoleucine, 0.23; leucine, 0.23; lysine hydrochloride, 0.42; methionine, 0.25; phenylalanine, 0.13; proline, 0.10; serine, 2.10; threonine, 0.23; tyrosine, 0.17; and valine, 0.23. The following L-amino acids were added by sterile filtration after the heat-sterilized medium had been cooled (g/L): tryptophan, 0.05; and, as appropriate, either the natural abundance or isotopically labeled forms of cysteine, 0.06; and histidine, 0.10.

For preparation of T4MOC selectively labeled in cysteine, the cells were grown and induced as described above for preparation of [*U*-^{15}N]-T4MOC. For two preparations of T4MOC selectively labeled with [^{2}H$^{\epsilon 1}$]His, the growth medium was supplemented with 17% (v/v) D_2O to prevent complete exchange of the isotopic label during growth and expression (*23*). For all preparations of T4MOC selectively labeled in histidine, the cell growths and expressions were performed in shaken flask culture as follows. A 50 mL culture of the amino acid supplemented minimal medium described above containing ampicillin (400 μg/mL) was inoculated with a single colony from an agar plate and grown to an OD_{600} of 0.1. This culture was used to inoculate eight 2 L flasks that each contained 500 mL of medium. The cultures were grown to an OD_{600} of ~2 and then induced by the addition of IPTG to a final concentration of 0.1 mM. After 5 h, the cells were harvested and stored as described above.

Purification of T4MOC. The frozen cell pellet (20−40 g) was thawed in a stainless steel beaker and resuspended in an equal volume of 25 mM MOPS, pH of 7.0, containing 2% (v/v) glycerol (buffer A). DNase (bovine pancreatic DNAse I, Sigma Chemical Co., St. Louis, MO), RNase (bovine pancreatic ribonuclease A; Sigma), and lysozyme (hen egg white; Sigma) (0.5 mg of each) were added to the suspension. The beaker was placed in an ice bath and sonicated for 5 min at maximum power output (Fisher model 550 sonic dismembrator, Pittsburgh, PA). The sonicated suspension was clarified by centrifugation at 43000*g* for 45 min. The supernatant was decanted, diluted with an equal volume of buffer A, and immediately loaded onto a DEAE fast-flow column (45 × 250 mm) equilibrated in buffer A. The column was washed with 2 column volumes of buffer A containing 0.15 M NaCl, and T4MOC was eluted with a 1.0 L linear gradient of 0.15 to 0.50 M NaCl in buffer A at 15 cm/h. Fractions containing T4MOC were identified by optical spectroscopy, pooled, and loaded onto a second DEAE column (25 × 80 mm) equilibrated in 25 mM MOPS, pH 7.4, containing 2% (v/v) glycerol (buffer B). T4MOC was eluted from the second DEAE column with a 1.0 L gradient of 0.20 to 0.55 M NaCl in buffer B at 5 cm/h. Fractions containing T4MOC were pooled and concentrated to ~3 mL using ultrafiltration (Amicon YM-3, Beverly, MA). The protein was then applied to a Sephacryl S-100 column (26 × 600 mm) equilibrated in 25 mM MOPS, pH 7.0, containing 5% (v/v) glycerol and 0.10 M NaCl and eluted at 6 cm/h. Fractions containing pure T4MOC were identified by optical spectroscopy ($A_{456}/A_{280} \geq 0.2$) and denaturing gel electrophoresis. The purified protein was concentrated by ultrafiltration and stored frozen at −80 °C until needed.

Preparation of NMR Samples. NMR solvents (D_2O and deuterium-depleted water) were obtained from Cambridge Isotope Labs. T4MOC samples were exchanged into the appropriate buffers using repeated cycles of dilution with the desired buffer and concentration by ultrafiltration. As indicated in the figure captions, [NA]T4MOC and T4MOC labeled with either ^{2}H ([^{2}H$^{\alpha}$]Cys, [^{2}H$^{\beta 2,\beta 3}$]Cys, [^{2}H$^{\epsilon 1}$]His) or ^{15}N ([*U*-^{15}N], [^{15}N]Cys, [^{15}N]His, [^{15}N$^{\delta 1}$]His, [^{15}N$^{\delta 1,\epsilon 2}$]His, [^{15}N]Ile, [^{15}N]Ala, [^{15}N]Gln) were exchanged into 50 mM phosphate in D_2O, pH 7.4* (pH measurements were not corrected for the deuterium isotope effect on the glass electrode). After buffer exchange, the samples were concentrated by ultrafiltration to 0.5−2.0 mM for NMR measurements. To prepare reduced samples, 2 mg of solid sodium dithionite was added to T4MOC samples made anaerobic in NMR tubes by repeated cycles of flushing with O_2-free Ar gas. The NMR tubes were then sealed by flame while under an Ar atmosphere.

NMR Spectroscopy. All ^{1}H and ^{2}H NMR spectra were collected on Bruker DMX400 wide-bore or DMX500 NMR spectrometers with either a 5 mm ^{1}H probe or a 10 mm broad-band probe. One-dimensional ^{15}N NMR spectra were recorded on a Bruker DMX600 NMR spectrometer with a 5 mm broad-band probe. A simple delay-90°-acquisition pulse sequence was used for all one-dimensional ^{1}H, ^{2}H, and ^{15}N experiments. Fast pulse repetition rates were used to saturate the more slowly relaxing diamagnetic resonances. ^{1}H chemical shifts were referenced to the methyl signal of 2,2-dimethylsilapentane-5-sulfonic acid, and the ^{2}H and ^{15}N chemical shifts were indirectly referenced to ^{1}H chemical shifts by multiplying the spectrometer frequency corresponding to 0 ppm in the ^{1}H spectrum by the ^{2}H/^{1}H (0.153 506 088) or the ^{15}N/^{1}H (0.101 329 118) frequency ratios, respectively (*22*). Other details of the data collection are provided in the table legends and figure captions.

A ^{1}H-^{13}C spectrum of [*U*-^{13}C]T4MOC was collected on a Bruker DMX500 spectrometer using a two-dimensional HMQC (*26*) experiment modified as jump-return echo sequence (*27*) for the suppression of water and the diamagnetic resonances. The anti-phase build-up period for the HMQC was 1.25 ms, and the excitation maximum for the jump-return sequence was centered at 25 ppm. The total recycle delay (relaxation delay and acquisition time) was 82 ms. The sweep width in the ^{1}H dimension was 100 ppm and in the ^{13}C dimension was 250 ppm. The data were collected as 256 rows of 4096 data points. ^{13}C decoupling was not applied during the acquisition period and thus the multiplet structure remains.

RESULTS

Expression and Characterization of T4MOC. The four proteins constitute comprise the enzyme complex encoded by the *tmoA-F* gene cluster were previously expressed in *E. coli* from vectors containing either the *lac* or *tac* promoters (*14*). Using these constructs, we produced and purified T4MOC and then performed physical characterizations and preliminary ^{1}H NMR measurements (*17*). The physical characterizations revealed that T4MOC had a high solubility without the addition of detergents, was stable in the pH range 6.0−10.5, and had long-term thermal stability at 30 °C. Moreover, the ^{1}H NMR studies revealed hyperfine-shifted resonances with short relaxation times and temperature dependences that were distinct from those previously observed for other [2Fe-2S] ferredoxins (see below). Therefore, selective isotopic labeling was used in the present study to classify these resonances.

To facilitate these labeling studies, an expression vector that allowed coexpression of T4MOC (12.3 kDa) and T4MOD (11.6 kDa) from a single T7 promoter in a pET-derived vector was developed (pJP01). This vector provided ~10−25 mg of pure T4MOC per liter of culture medium, which represented an increase in yield of ~10-fold relative to expression from the complete *tmoA-F* gene cluster in the

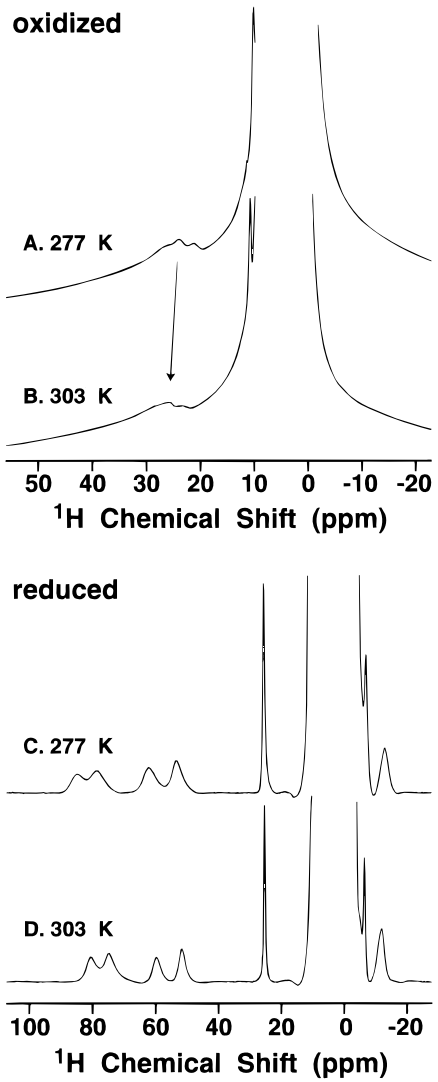

FIGURE 2: ^{1}H NMR signals from [NA]T4MOC in ^1H_2O. Oxidized T4MOC: (A) 277 K; (B) 303 K. Reduced T4MOC: (C) 277 K; (D) 303 K.

previously used pUC-derived vectors. Physical (optical, EPR, metal content) and catalytic characterizations (~15 units/mg for *p*-cresol formation in the presence of optimal concentrations of the other T4MO components) revealed that T4MOC obtained from pJP01 was indistinguishable from previously characterized preparations (*14*).

Nucleotide sequencing of the coding region of pJP01 confirmed that T4MOC contains five Cys residues (C7, C45, C64, C84, and C85, with C45 and C64 present in the metal-binding motif) and five His residues (H36, H47, H67, H77, and H111, with H47 and H67 present in the metal-binding motif). The nuclei associated with the Cys and His ligands are expected to have paramagnetic behavior, while the nuclei associated with the remaining Cys and His are likely to have diamagnetic behavior.

^{1}H NMR Studies of T4MOC. Figure 2 shows one-dimensional ^{1}H NMR spectra of T4MOC in the oxidized and reduced states, respectively, while Table 1 lists the chemical shifts and classification of the hyperfine-shifted resonances observed in these spectra. In the ^{1}H NMR spectra of *oxidized* T4MOC (Figure 2, panels A and B), broad signals were observed in the high-frequency region from 20 to 30 ppm and a relatively sharp signal was observed at 10.7 ppm. All of these signals exhibited anti-Curie temperature dependence (shifts to high frequency, away from the diamagnetic region with increasing temperature; 0.038 to 0.077 ppm/K). After exchange into ^2H_2O, no change in the intensity of these signals was observed (data not shown).

In the ^{1}H NMR spectra of *reduced* T4MOC, four broad peaks, each of ~1 proton intensity, were observed in the high-frequency region between 50 and 90 ppm (chemical shifts of 82.7, 76.7, 61.1, and 52.6 ppm at 293 K; Figure 2, panels C and D, Table 1). Each of these resonances exhibited strong Curie temperature dependence (shifts to low frequency, toward the diamagnetic region with increasing temperature; −0.065 to −0.161 ppm/K). The magnitudes of the temperature dependences of the chemical shifts observed for these resonances are comparable to those previously observed for Cys H^β of plant-type [2Fe-2S] ferredoxins (*28*). A relatively sharp peak accounting for ~1 proton was also observed at 25.5 ppm, in a spectral region reminescent of where the H^α protons of the Cys ligands of the plant-type ferredoxins appear. However, the Curie temperature dependence of this peak was substantially smaller (−0.010 ppm/K) than that observed for any resonances assigned to Cys H^α bound to the localized ferric site in reduced *Anabaena* (−0.10 ppm/K for C49 and −0.05 ppm/K for C79), spinach (−0.17 ppm/K), or vertebrate (−0.10 ppm/K) [2Fe-2S] ferredoxins (*25*, *29*−*33*).

In the low-frequency region of the ^{1}H NMR spectra of *reduced* T4MOC, two peaks, each of ~1 proton intensity, were observed near the diamagnetic shoulder at −6.6 ppm and at −12.3 ppm (Figure 2, panels C and D, Table 1). These peaks exhibited weak pseudo-Curie temperature dependence (shifts to high frequency, toward the diamagnetic region with increasing temperature; 0.019 and 0.038 ppm/K, respectively). As described below, the hydrogen giving rise to the −12.3 ppm resonance is solvent exchangeable preferentially when T4MOC is in the oxidized state, whereas the −6.6 ppm resonance is not exchangeable. In the plant-type [2Fe-2S] ferredoxins, ^{1}H resonances in the low-frequency region have been associated only with solvent-exchangeable nuclei, while in contrast, both exchangeable and nonexchangeable ^{1}H resonances with Curie temperature dependence have been observed from the vertebrate ferredoxin in the low-frequency region.

The presence of ^{1}H resonances shifted to both high and low frequency of the diamagnetic region in the reduced Rieske proteins is unique when compared to the plant-type and vertebrate [2Fe-2S] ferredoxins (*18*, *33*). Although the five nonexchangeable resonances at highest frequency in *reduced* T4MOC have a pattern similar to that observed from the H^β and H^α protons of the Cys ligands in the plant-type ferredoxins (*25*), the temperature dependence of the H^α-like peak is anomalous. Furthermore, the two low-frequency resonances in *reduced* T4MOC are most similar to those observed in the vertebrate ferredoxin (*34*), which clearly does not contain His ligands to the [2Fe-2S] center or H-bonding from His nitrogen nuclei (*24*, *34*). One-dimensional ^{1}H-^{1}H NOE spectra of T4MOC did not reveal connectivities between the hyperfine-shifted peaks in the high-frequency region between 50 and 90 ppm and the 25.5 ppm peak or the low-frequency region at −6.6 ppm and at −12.3 ppm; similar negative NOE results have been found for vertebrate [2Fe-2S] ferredoxins (*34*). The lack of NOEs is presumably

Table 1: Chemical Shifts, Temperature Dependence, and Classification of Hyperfine-Shifted ^{1}H and ^{2}H Resonances of the Rieske Ferredoxin Component of Toluene 4-Monooxygenase

	oxidized state			reduced state		
	chemical shift[a] (ppm)	temperature dependence[b] (Δppm/K)	classification	chemical shift[a] (ppm)	temperature dependence[b] (Δppm/K)	classification
^{1}H	10.7	0.038				
	20−30	0.077	C45 $H^{\beta2,\beta3}$/C64 $H^{\beta2,\beta3}$	82.7/76.7/61.1/52.6	−0.161/−0.148/−0.092/−0.065	C45 $H^{\beta2,\beta3}$/C64 $H^{\beta2,\beta3}$
				25.5	−0.010	H47 $H^{\epsilon1}$ or H67 $H^{\epsilon1}$
				−6.6	0.019[d]	
				−12.3[c]	0.038[d]	peptidyl or imidazole N−H
^{2}H						
	20−30	0.077	C45 $H^{\beta2,\beta3}$/C64 $H^{\beta2,\beta3}$	∼80/∼60	<0	C45 $H^{\beta2,\beta3}$/C64 $H^{\beta2,\beta3}$
				∼25	nd[e]	H47 $H^{\epsilon1}$ or H67 $H^{\epsilon1}$

[a] Chemical shifts at 293 K. [b] Change in chemical shift as a function of temperature in the range 277−303 K. Temperature was controlled to ±1 K. [c] Lost after exchange into ^2H_2O buffer and incubation for ca. 2 days in the oxidized state. Incubation in the reduced state for as long as 30 days gave no detectable exchange (see Figure 3A). [d] Low frequency resonances shifted toward the diamagnetic region with increasing temperature. [e] nd, not determined due to weak signal intensity in [$^2H^{\epsilon1}$]His T4MOC.

due to the rapid relaxation rate for the protons in T4MOC. Thus, selective isotopic labeling was used to ascertain the origin of the ^{1}H NMR signals from T4MOC.

NMR Studies of T4MOC Labeled Selectively with ^{2}H. One-dimensional ^{2}H NMR spectra of oxidized and reduced T4MOC selectively labeled by incorporating [$^2H^{\alpha}$]Cys, [$^2H^{\beta2,\beta3}$]Cys, and [$^2H^{\epsilon1}$]His are shown in Figure 3. The Cys selective labelings were performed in an *E. coli* strain lacking *O*-acetylserine transferase, encoded by the *cysE* gene. In principle, *O*-acetylserine (thiol) lyase (*cysK* gene product) could catalyze exchange of exogenously added [$^2H^{\alpha}$]Cys (*35*); however, expression of the *cysE* and *cysK* genes is strongly repressed in the presence of cysteine or sulfide (*36*). Although isotopic exchange at the H^{α} positions of some amino acid residues has been detected during expression of proteins for NMR studies (*35*), it has not been observed at the Cys H^{α} position by using *E. coli* JM15 *(cysE50, tfr-8)* for numerous growth, expression, and purification experiments with other iron−sulfur proteins such as rubredoxin (*37*) and ferredoxins (*24*, *32*, *33*, *38*).

In the ^{2}H NMR spectra of both *oxidized* and *reduced* [$^2H^{\alpha}$]-Cys T4MOC, no hyperfine-shifted resonances were observed outside of the region obscured by the water peak (Figure 3, panels B and F, respectively). Furthermore, none of the observed hyperfine-shifted peaks were missing in the ^{1}H NMR spectra of oxidized and reduced [$^2H^{\alpha}$]Cys T4MOC; these spectra (not shown) were identical to those of [NA]-T4MOC. Since Resonance Raman studies[2] of the same [$^2H^{\alpha}$]-Cys T4MOC preparations revealed mass-dependent frequency shifts of −0.5 to −1.1 cm^{-1} in the bands assigned to vibrations of the Fe−S−Cys terminal ligands, ^{2}H was confirmed to be present in the [$^2H^{\alpha}$]Cys T4MOC used for the NMR studies. Thus, unlike the H^{α} nuclei of the Cys ligands of plant-type [2Fe-2S] ferredoxins, the H^{α} nuclei of the Cys ligands of T4MOC Rieske ferredoxin do not exhibit hyperfine shifts large enough so that their signals can be resolved from the diamagnetic region.

For *oxidized* T4MOC labeled with [$^2H^{\beta2,\beta3}$]Cys, a broad peak was observed in the high-frequency region of the one-dimensional ^{2}H NMR spectrum between 20 and 30 ppm (Figure 3C) with chemical shift and anti-Curie temperature dependence equivalent to the corresponding ^{1}H NMR peaks of [NA]T4MOC (Figure 3A). Therefore, these high-frequency peaks in the ^{1}H NMR spectra of oxidized T4MOC have been assigned to the four β-protons of C45 and C64, the two cysteines that are found in the T4MOC Rieske center metal binding motif (Table 1).

For *reduced* T4MOC labeled with [$^2H^{\beta2,\beta3}$]Cys, two broad peaks were observed in the ^{2}H NMR spectrum at 283 K (Figure 3G). Both of these peaks exhibited Curie temperature dependence, and at 303 K, the two broad peaks were partially resolved into two sets of doublets (data not shown). The chemical shifts of the four peaks resolved at 303 K (50−90 ppm) were nearly identical to those of the four peaks observed in the natural abundance sample. The labeling results establish that these peaks arise from the four β protons of the two ligand cysteines (C45 and C64, Table 1).

To further investigate ^{1}H resonances from the His ligands, a sample of T4MOC selectively labeled with [$^2H^{\epsilon1}$]His was produced by growing the His-auxotrophic expression host *E. coli* AW608Thr$^+$T7/pLysS in a minimal medium containing >90% enriched [$^2H^{\epsilon1}$]His (Figure 3, panels D and H). This auxotroph has been reliably used in numerous labeling studies and there has been no evidence for scrambling of atoms on labeled His. The sample of Figure 3, panels D and H, had a protein concentration (∼1 mM) similar to the samples used to obtain all of the other spectra shown in Figure 3. The ^{2}H NMR spectrum of *oxidized* [$^2H^{\epsilon1}$]His-T4MOC showed no hyperfine-shifted signals resolved from the broad water peak (Figure 3D). In the *reduced* state, ^{2}H NMR revealed a broad, weak shoulder at ∼25 ppm (indicated by the arrow in Figure 3H). This shoulder had a chemical shift similar to the relatively sharp peak at 25.5 ppm in the ^{1}H NMR spectrum of reduced [NA]-T4MOC (Figure 3E).

Since His $H^{\epsilon1}$ represents the only carbon-bound hydrogen that readily undergoes abiotic exchange with solvent-derived H (*39*), the low intensity of the hyperfine-shifted His $H^{\epsilon1}$ peak in Figure 3H may have resulted from chemical exchange of [$^2H^{\epsilon1}$]His during the cell growth and expression procedures (*23*). To further test the proposed assignment of the 25.5 ppm peak to His $H^{\epsilon1}$, another sample of [$^2H^{\epsilon1}$]His T4MOC was produced by growing the His-auxotrophic expression host in a minimal medium supplemented with

[2] F. Rotsaert, J. D. Pikus, B. G. Fox, J. L. Markley, and J. Sanders-Loehr, unpublished data.

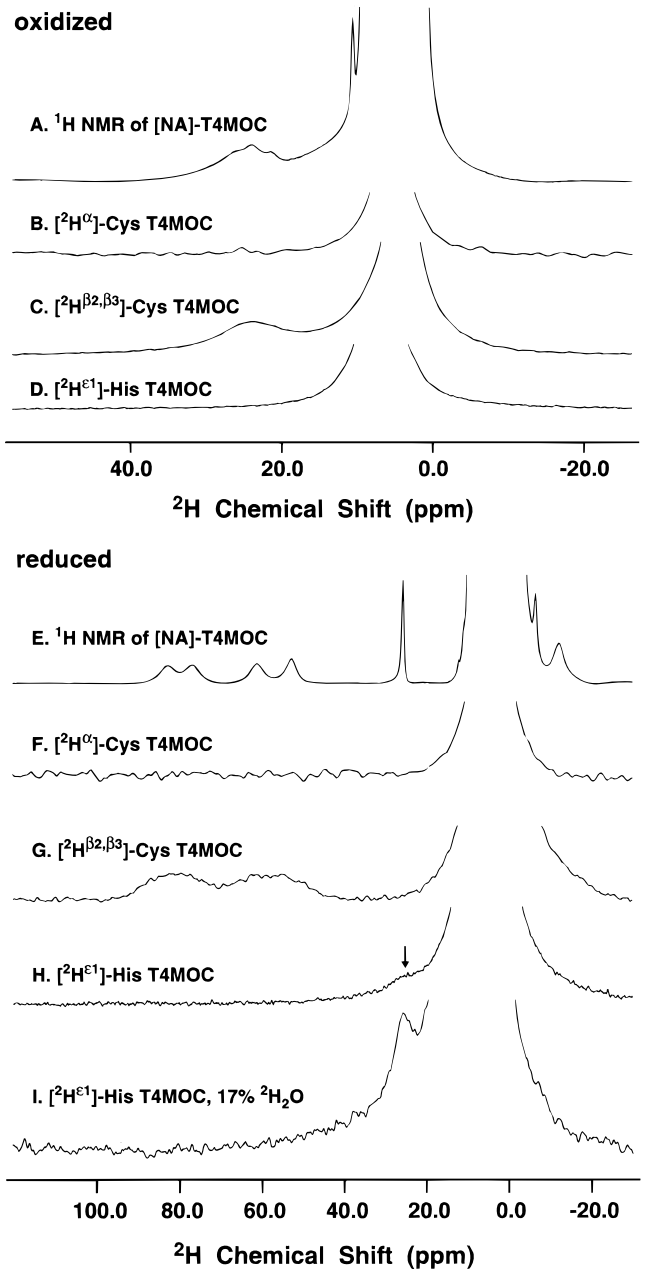

FIGURE 3: ^{2}H NMR signals observed from selectively labeled T4MOC. Oxidized T4MOC: (A) ^{1}H NMR of [NA]T4MOC; (B) [^{2}H$^{\alpha}$]Cys; (C) [^{2}H$^{\beta2,\beta3}$]Cys; (D) [^{2}H$^{\epsilon1}$]His. Reduced T4MOC: (E) ^{1}H NMR of [NA]T4MOC; (F) [^{2}H$^{\alpha}$]Cys; (G) [^{2}H$^{\beta2,\beta3}$]Cys; (H) [^{2}H$^{\epsilon1}$]-His expressed in H_2O medium; (I) [^{2}H$^{\epsilon1}$]His expressed in medium containing 17% ^2H_2O. All spectra shown were obtained at 293 K.

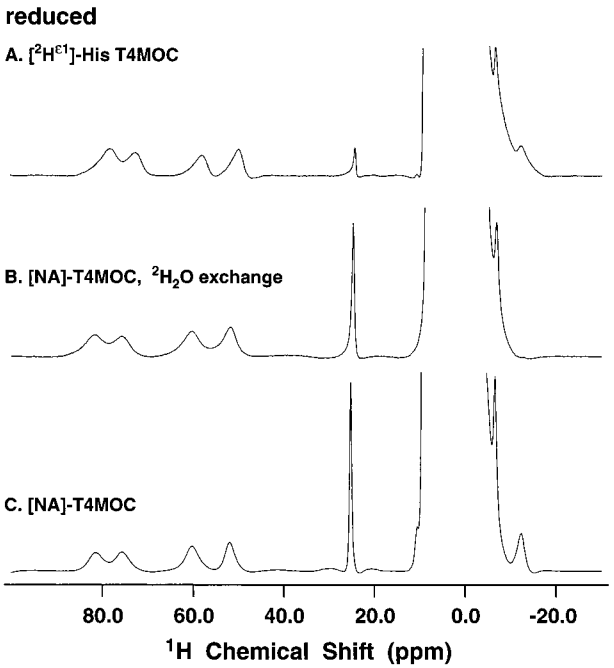

FIGURE 4: ^{1}H NMR signals observed from reduced T4MOC selectively labeled with [^{2}H$^{\epsilon1}$]His or at natural abundance. (A) [^{2}H$^{\epsilon1}$]-His T4MOC expressed in a minimal medium containing 17% (v/v) ^2H_2O and purified in H_2O buffers as described in the Materials and Methods. (B) A sample of oxidized [NA]His T4MOC exchanged into ^2H_2O and then incubated for ca. 2 days at room temperature before reduction; (C) [NA]T4MOC.

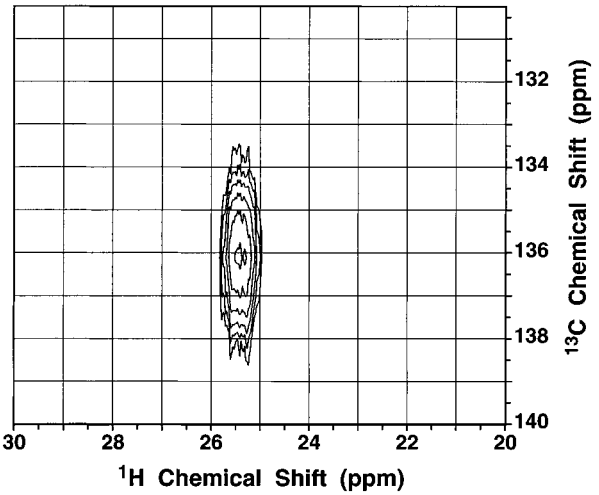

FIGURE 5: ^{1}H-^{13}C heteronuclear multiple quantum correlation spectrum of reduced [U-^{13}C]T4MOC.

>95% enriched [^{2}H$^{\epsilon1}$]His and 17% (v/v) ^2H_2O. ^{1}H NMR was then used to measure the intensity of the 25.5 ppm peak in this sample (Figure 4A). The ^{1}H measurement revealed that the 25.5 ppm peak had roughly 15% of the intensity of the corresponding peak of [NA]T4MOC (Figure 4C). This decrease in intensity of the ^{1}H signal is consistent with the deliberate substitution of ^{2}H into the H$^{\epsilon1}$ position of the labeled histidine used to grow the auxotroph. Moreover, the ^{2}H NMR spectrum of [^{2}H$^{\epsilon1}$]His T4MOC expressed in 17% ^2H_2O (Figure 3I) showed a substantial increase in the intensity at 25.5 ppm relative to the sample prepared without supplemented ^2H_2O (Figure 3H). Continued incubation of the [^{2}H$^{\epsilon1}$]His T4MOC sample in ^1H_2O buffer for ca. 1 month at 4 °C allowed exchange of ^{2}H and complete restoration of the 25.5 ppm peak in the ^{1}H NMR spectrum (data not shown).

Additional evidence that the 25 ppm peak arises from His H$^{\epsilon1}$ comes from the detection of a cross-peak in the two-dimensional ^{1}H-^{13}C HMQC spectrum of [*U*-^{13}C]T4MOC at 25.39 ppm ^{1}H and 136.11 ppm ^{13}C (Figure 5). This ^{13}C chemical shift is close to the value expected for a positively charged His ^{13}C$^{\epsilon1}$ (~137 ppm). Furthermore, the ^{1}H-^{13}C coupling constant for this pair (189−195 Hz) is consistent with that for a histidine or aromatic CH (180−220 Hz), but not with that for an aliphatic CH such as Cys H$^{\alpha}$-C$^{\alpha}$ (~140 Hz). Thus, taken together, the isotopic labeling and exchange results of Figures 3 and 4 and the two-dimensional ^{1}H-^{13}C HMQC spectrum of Figure 5 provide compelling evidence

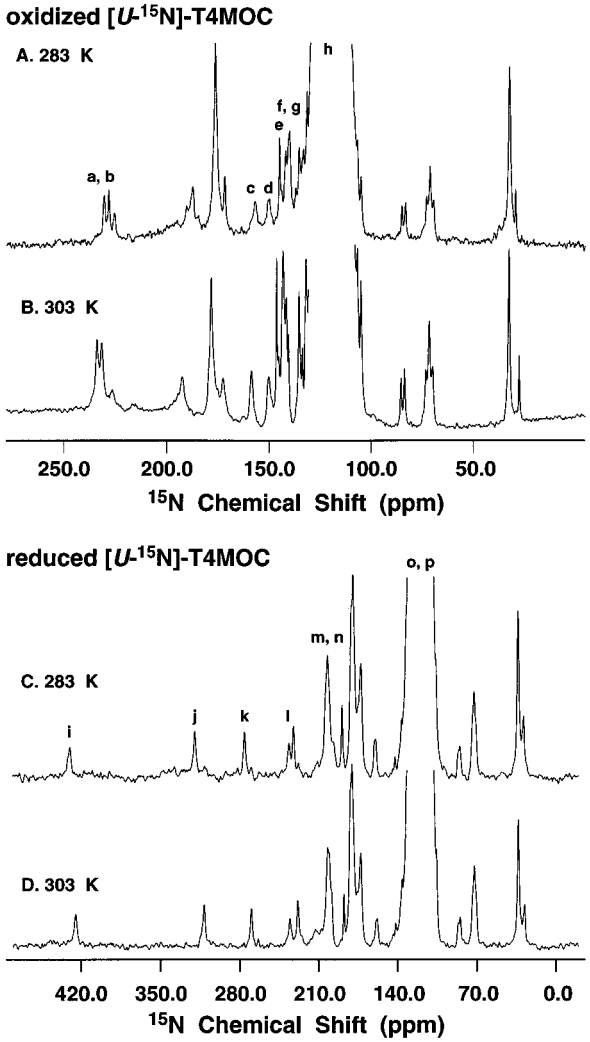

FIGURE 6: Temperature dependence and classification of ^{15}N NMR signals of [U-^{15}N]T4MOC. Oxidized T4MOC: (A) 283 K; (B) 303 K. Reduced T4MOC: (C) 283 K; (F) 303 K. The letters assigned to individual resonances correspond to those used in Table 2.

that the 25.5 ppm resonance in T4MOC arises from the $H^{\epsilon 1}$ proton of one of the histidines ligated to the Rieske cluster (H47 or H67).

Figure 4B shows that the −12.3 ppm resonance was the only resolved hyperfine-shifted ^1H signal in *reduced* T4MOC that exchanged completely with solvent-derived ^2H. However, it is notable that whereas this exchange took ca. 2 days at room temperature to reach completion when T4MOC was in the oxidized state, no measurable exchange took place at this position when T4MOC was in the reduced state, even after 2 weeks of anaerobic incubation at 4 °C followed by an additional 2 weeks of anaerobic incubation at room temperature. The exchange results suggest that the −12.3 ppm resonance of T4MOC arises from a group that donates a strong H-bond to the Rieske cluster and that the strength of this bond is substantially stronger (or its solvent accessibility is considerably lower) in the reduced state than in the oxidized state.

^{15}N NMR Spectra of T4MOC Cluster Ligands. Figure 6 shows one-dimensional ^{15}N NMR spectra of [*U*-^{15}N]T4MOC in the oxidized and reduced states, while Table 2 lists the chemical shifts, temperature dependences, and classifications of the hyperfine-shifted ^{15}N resonances identified in these spectra.

Figure 7 compares the one-dimensional ^{15}N NMR spectra of oxidized and reduced T4MOC labeled selectively with ^{15}N. The ^{15}N spectrum of *oxidized* [$^{15}N^{\delta 1,\epsilon 2}$]His T4MOC contained a broad spectral feature corresponding to the diamagnetic [$^{15}N^{\delta 1,\epsilon 2}$]His resonances at ∼170 ppm and two hyperfine-shifted resonances with slightly inequivalent chemical shifts at 233.8 and 231.5 ppm (Figure 7A, resonances *a* and *b)*. The hyperfine-shifted resonances exhibited weak anti-Curie temperature dependence. In the *reduced* state, the ^{15}N resonances assigned to the diamagnetic His residues remained at ∼170 ppm, while the two hyperfine-shifted resonances appeared ∼120 ppm to lower frequency at 119.7 and 116.3 ppm (Figure 7A, resonances *o* and *p)*. These two hyperfine-shifted resonances exhibited weak pseudo-Curie temperature dependence. While the ^{15}N NMR spectra of both the oxidized and reduced states of T4MOC selectively labeled with [$^{15}N^{\delta 1}$]-His did not exhibit hyperfine-shifted resonances (data not shown), resonance Raman studies[2] of [$^{15}N^{\delta 1}$]His T4MOC revealed mass-dependent frequency shifts in the bands assigned to the Fe−N (imidazole) vibrations. These shifts were comparable to the shifts observed from [*U*-^{15}N]T4MOC, confirming that ^{15}N was present in the [$^{15}N^{\delta 1}$]His T4MOC used for the NMR studies, and supporting the assignment that the [$^{15}N^{\delta 1}$] position of His is bonded to iron in T4MOC. Therefore, the ^{15}N signals marked in Figure 7A (resonances a and b, o and p) have been classified to arise from the $N^{\epsilon 2}$ position of cluster ligands H47 and H67 in the oxidized and reduced states, respectively. Apparently, the signals from the $N^{\delta 1}$ atom of each His are both too broad to be detected under the experimental conditions used.

The ^{15}N NMR spectra of oxidized and reduced [^{15}N]His T4MOC are shown in Figure 7B. Five resolved ^{15}N signals were observed in both the oxidized and the reduced states, corresponding to the five His residues present in T4MOC. In the *oxidized* state, one resonance was distinct from the other four (Figure 7B, resonance c). This resonance was shifted to high frequency from the diamagnetic region (158.7 ppm) and had weak anti-Curie temperature dependence. The other four resonances were at ∼120 ppm. In the *reduced* state, the ^{15}N resonances from two of the five His residues underwent a shift to high frequency and were observed at 304.2 ppm (resonance j) and 270.3 ppm (resonance k). Both of these peaks exhibited Curie temperature dependence. The hyperfine-shifted ^{15}N resonances marked in Figure 7B (resonances c and h, j and k) are thus classified to arise from the amide nitrogens of cluster ligands H47 and H67 in the oxidized and reduced states, respectively.

The ^{15}N NMR spectra of oxidized and reduced [^{15}N]Cys T4MOC are shown in Figure 7C. The unresolved peak at ∼110 ppm in both redox states (largely saturated under the conditions used to detect the hyperfine-shifted signals) is attributed to diamagnetic ^{15}N resonances from the three nonligand Cys residues. In the *oxidized* state, two hyperfine-shifted resonances with slightly inequivalent chemical shifts were observed at 143.5 ppm (resonance f) and 142.1 ppm (resonance g), just outside of the diamagnetic region (see Figure 6A). These resonances had weak anti-Curie temperature dependence. In the *reduced* state, these two resonances underwent a 60 ppm shift toward higher frequency and appeared at 201.8 ppm (resonance m) and 200.6 ppm (resonance n). Each of these resonances had Curie temperature dependence. The hyperfine-shifted ^{15}N resonances

Table 2: Chemical Shifts, Temperature Dependence, and Classification of Hyperfine-Shifted ^{15}N Resonances of the Rieske Ferredoxin Component of Toluene 4-Monooxygenase

	oxidized state				reduced state		
peak[a]	chemical shift[b] (ppm)	temperature dependence[c] ($\Delta\delta/\Delta T$)	classification or assignment	peak[a]	chemical shift[b] (ppm)	temperature dependence[c] ($\Delta\delta/\Delta T$)	classification or assignment
a, b	233.8/231.5	>0[d]	H47 N$^{\epsilon 2}$/H67 N$^{\epsilon 2}$	o, p	119.7/116.3	nd[e]	H47 N$^{\epsilon 2}$/H67 N$^{\epsilon 2}$
c, h	158.7/122.6	>0	H47 N/H67 N	j, k	304.2/270.3	<0	H47 N/H67 N
d	150.6	~0	A66 N	l	228.6	<0	A66 N
e	141.4	>0	Q48 N	i	426.1	<0	Q48 N
f, g	143.5/142.1	>0	C45 N/C64 N	m, n	201.8/200.6	<0	C45 N/C64 N

[a] Peaks as indicated in Figures 5, 6, and 7. [b] Chemical shifts at 293 K. [c] Change in chemical shift as a function of temperature in the range 283−303 K. Temperature was controlled to ±1 K. [d] Temperature dependence of signals *a* and *b* determined from study of [U-^{15}N]T4MOC. [e] nd, not determined due to weak intensity of signals *o* and *p* in [^{15}N$^{\delta 1,\epsilon 2}$]His T4MOC.

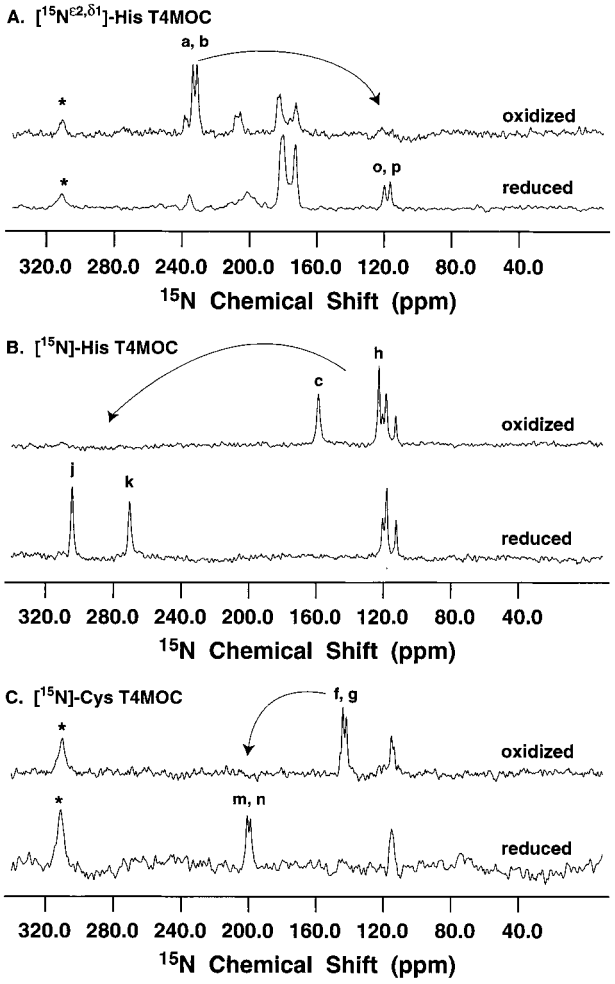

FIGURE 7: Comparison of ^{15}N chemical shifts T4MOC selectively labeled with ligand amino acids upon conversion from the oxidized to the reduced state. (A) [^{15}N$^{\delta 1,\epsilon 2}$]His; (B) [^{15}N]His; (C) [^{15}N]Cys. The peaks indicated (*) in panels A and C arise from natural abundance ^{15}N^{14}N gas in air. All spectra shown were obtained at 293 K.

marked in Figure 7C (resonances f and g, m and n) are thus assigned to the backbone nitrogens of cluster ligands C45 and C64 in the oxidized and reduced states, respectively.

^{15}N NMR Spectra of T4MOC Residues Potentially Involved in H-Bonding to the Rieske Cluster. The network of H-bonding to the Rieske cluster observed in the ISP crystal structure (Figure 1) was used to identify candidate residues for the hyperfine-shifted ^{15}N resonances to be verified by ^{15}N labeling. The residues in T4MOC that correspond to

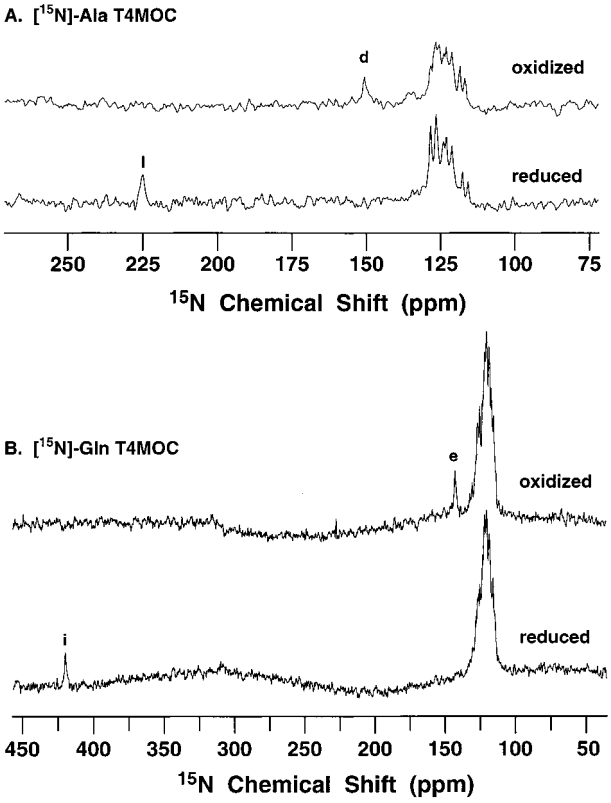

FIGURE 8: Comparison of ^{15}N chemical shifts in T4MOC selectively labeled with hydrogen bonding amino acids upon conversion from the oxidized to the reduced state. (A) [^{15}N]Ala; (B) [^{15}N]Gln. All spectra shown were obtained at 293 K.

those whose backbone H^N atoms donate H-bonds are H47, H67, Q48, I50, and A66, with I50 and A66 at the positions of the Cys residues that form a disulfide bond in the ISP structure. The NMR spectra of [^{15}N]Ile T4MOC did not contain paramagnetically shifted resonances in either the oxidized or reduced states, suggesting that the amide group of I50 is not strongly H-bonded to the T4MOC Rieske cluster. Figure 8A shows ^{15}N NMR spectra of [^{15}N]Ala T4MOC. In the *oxidized* state, a single hyperfine-shifted resonance was observed at 150.6 ppm with anti-Curie temperature dependence, while in the *reduced* state, this resonance shifted to 228.6 ppm and had Curie temperature dependence.

Figure 8B shows ^{15}N NMR spectra of [^{15}N]Gln T4MOC. In the *oxidized* state, a single hyperfine-shifted resonance was observed at 141.4 ppm with anti-Curie temperature dependence, while in the *reduced* state, this resonance shifted

to 426.1 ppm and had Curie temperature dependence. Thus, ^{15}N NMR reveals that two of the three nonligand peptidyl N−H bonds observed in the ISP domain are also conserved in T4MOC.

DISCUSSION

Methodology Used for Investigating the Delocalization of Unpaired Electrons in T4MOC. Of the general methods used for assigning NMR signals of proteins (through-space nuclear Overhauser effect connectivities, through-bond *J*-coupling connectivities and selective isotope labeling), only stable isotope labeling provides unambiguous results for strongly paramagnetic systems whose lines are too broad to yield interpretable NOE and *J*-coupling effects. In addition to assisting with assignments, low magnetogyric nuclei (^{2}H and ^{15}N) introduced by labeling can serve as reporters for specific interactions between nuclei and unpaired electrons (*25*, *33*). Therefore, we have focused this work on the study of T4MOC samples prepared with ^{2}H or ^{15}N labels in defined positions through the use of well-characterized, reliable auxotrophic expression hosts.

Comparison of the Present ^{1}H NMR Results for T4MOC with Those Reported Recently for the Related Rieske Protein from Xanthobacter. T4MOC and the Rieske protein from *Xanthobacter* studied by Holz and co-workers (*18*) are intermediate electron carriers to evolutionarily related diiron hydroxylase complexes (*40*). Moreover, they exhibit similar optical and EPR properties, consistent with the presence of the Rieske protein metal-binding motif shown in Figure 1. Thus, while no exact sequence information is available for the *Xanthobacter* Rieske protein, it and T4MOC may be expected to exhibit a very similar cluster environment and pattern of hyperfine-shifted resonances. Although no data are available on the ^{15}N signals of the *Xanthobacter* Rieske protein, the pattern of ^{1}H NMR signals in the *Xanthobacter* Rieske protein (*18*) are nearly identical to those of T4MOC (*17*). Despite these similarities, fundamental differences exist between some of the peak identifications made by Holz and co-workers (*18*) and those made here for signals from the Cys and His residues that ligate the T4MOC Rieske cluster. Therefore, it is important to address these differences before proceeding with the discussion of the results.

The two studies are in agreement in attributing the four peaks in the 50−90 ppm region of the reduced Rieske proteins to the $H^{\beta2,\beta3}$ protons of the two cysteines ligating the cluster; for the *Xanthobacter* Rieske protein, this identification came primarily from comparisons with published spectra of plant-type ferredoxins. The NOE experiments Holz and co-workers used for additional assignments (*18*) suffered from apparent flaws; for example, the reported NOE signals were smaller than other (unexplained) peaks in the NOE difference spectra. Where differences occur, the peak identifications reported here [which rely on (1) rigorous isotopic labeling (Figure 3); (2) the unique ability of His $H^{\epsilon1}$ to undergo solvent exchange under mild conditions (*23*, *39*) (Figures 3 and 4); and (3) two-dimensional ^{1}H-^{13}C HMQC measurements (Figure 5)] would appear to take precedence over the previous assignment, which relied on the less rigorous methods of cross relaxation and assignment by analogy to results with plant-type ferredoxins. Thus, the present ^{1}H and ^{2}H NMR results with [$^2H^\alpha$]Cys T4MOC appear to invalidate the assignment of the sharp signals at ∼10 and ∼25 ppm in the ^{1}H spectra of the *Xanthobacter* Rieske protein to Cys H^α. Instead, it is likely that the peak at ∼25 ppm in the *Xanthobacter* Rieske protein arises from the $H^{\epsilon1}$ of one of the His ligands, as has been determined for T4MOC on the basis of ^{1}H and ^{2}H NMR data from selectively labeled protein samples (see Figures 3, 4, and 5).

The identifications of other signals in the −0.1 to −15.5 ppm region of ^{1}H NMR spectra of reduced *Xanthobacter* Rieske protein to the H^α, $H^{\beta2,\beta3}$, and $H^{\epsilon2}$ atoms of the two histidine ligands (*18*) must be viewed with circumspection until they can be confirmed by selective isotopic labeling. Of these signals, only two were clearly seen in ^{1}H NMR spectra of reduced T4MOC (Figure 2, bottom); that at the lower frequency (−12.3 ppm) was the only hyperfine-shifted ^{1}H signal from a hydrogen observed to undergo exchange with solvent. As shown here, hydrogen exchange at this position occurred at an appreciable rate only in the oxidized state of T4MOC. Similar redox state-dependent ^{1}H/^{2}H exchange has been reported for other ferredoxins (*41*−*43*). It would be interesting to determine if this is the case with the exchangeable hydrogens of the *Xanthobacter* Rieske protein that yield hyperfine shifts (*18*). A signal was not observed in spectra of T4MOC analogous to the second hyperfine-shifted ^{1}H resonance from *Xanthobacter* Rieske protein reported to be a solvent exchangeable site (*18*).

^{1}H and ^{2}H NMR Studies of T4MOC. In their oxidized states, both the plant-type and the vertebrate [2Fe-2S] ferredoxins exhibit broad hyperfine-shifted ^{1}H resonances between 20 and 40 ppm that have been assigned to the eight $H^{\beta2,\beta3}$ nuclei of the Cys ligands (*25*, *32*, *34*). Furthermore, ^{1}H signals at 9 and 15 ppm in spectra of oxidized plant-type ferredoxins have been assigned to the H^α nuclei of the two Cys ligands (*25*). The ^{1}H NMR spectrum of oxidized T4MOC has a high frequency pattern qualitatively similar to the plant-type ferredoxins in that a broad resonance with anti-Curie temperature dependence has been assigned to Cys $H^{\beta2,\beta3}$ by isotopic labeling (Figures 1 and 2, Table 1). The origin of the other hyperfine-shifted peak at 10.7 ppm has not been identified; however, Cys H^α can clearly be eliminated from consideration based on the [$^2H^\alpha$]Cys labeling study (Figure 3B).

In the reduced plant-type *Anabaena* ferredoxin, the $H^{\beta2,\beta3}$ nuclei of cluster ligands C49 and C79 give rise to a characteristic pattern of four high-frequency resonances between 98 and 135 ppm, while the H^α nuclei of these residues yield signals at 16.7 and 43.5 ppm; no low-frequency shifted resonances are observed from carbon-bound hydrogens. The ^{1}H NMR spectra of reduced T4MOC (Figure 2) also exhibit four hyperfine-shifted resonances at high frequencies (∼50 ppm to ∼80 ppm), which are similar to those observed from the $H^{\beta2,\beta3}$ atoms of the cysteines ligated to the localized ferric site in reduced plant-type ferredoxins (*25*, *44*). However, the ^{1}H NMR spectra of reduced T4MOC differ from those of the reduced plant-type ferredoxins in that no hyperfine-shifted Cys H^α resonances have been observed. Instead, the $H^{\epsilon1}$ proton of one His ligand (either H47 or H67) was identified in a relatively similar region of the high-frequency spectrum. The potential for hyperfine interactions at His $H^{\epsilon1}$ is supported by the observation that this nucleus is three bonds distant from the iron, the same number of

bonds as the hyperfine-shifted $H^{\beta 2,\beta 3}$ and $N^{\epsilon 2}$ nuclei. By contrast, the Cys H^{α}, His $H^{\beta 2}$, and $H^{\beta 3}$ atoms are four bonds from the nearest iron, and the His H^{α} atoms are six bonds distant. These latter nuclei are predicted to have smaller hyperfine shifts.

For the reduced [2Fe-2S] ferredoxins, the temperature dependence of the chemical shift has been widely used to identify the local spin system to which a given nucleus is bound (*18*, *28*, *44*). Thus, ^{1}H nuclei from Cys bound to the ferric site have Curie temperature dependence while ^{1}H nuclei from Cys bound to the ferrous site have anti-Curie temperature dependence. In the case of the Rieske protein, the hyperfine-shifted Cys H^{β} nuclei behave as previously observed in the plant-type [2Fe-2S] ferredoxins, with anti-Curie temperature dependence in the oxidized state and Curie temperature dependence in the reduced state. A similar comparison is not possible for the Cys H^{α} of T4MOC since signals from these nuclei were not observed. However, the $H^{\epsilon 1}$ nucleus of one His ligand (ligated to the ferrous site) has a weak Curie temperature dependence instead of the anti-Curie temperature dependence predicted from the simple vector coupling model. This deviation from the predicted temperature dependence is also observed for nitrogen atoms in the Rieske protein (Table 2) as well as nitrogen and carbon atoms in *Anabaena* ferredoxin (*25*). Taken together, these results suggest that a more refined theory needs to be developed to account for the experimental data, and that caution must be exercised when using the temperature dependence of hyperfine shifts to assign signals other than H^{β} and H^{α} of cysteine ligands to the localized ferric and ferrous sites of [2Fe-2S] ferredoxins.

^{15}N NMR Studies. In both the oxidized and reduced states, two hyperfine-shifted ^{15}N resonances were observed from [^{15}N]Cys T4MOC and from [^{15}N]His T4MOC. Thus, the peptidyl N^{α} atoms of each of the Cys and His ligands to the Rieske [2Fe-2S] cluster (C45, H47, C64, and H67) have distinct magnetic environments. This assessment is particularly evident from examination of the His amide nitrogen signals (Figure 7B). In the oxidized state, one ligand resonance is shifted by 40 ppm toward higher frequency from the diamagnetic region (resonance c), while the other ligand resonance (resonance h) has a chemical shift similar to the diamagnetic His backbone amide resonances. Upon reduction, both of these resonances (j and k) exhibit shifts to higher frequency that clearly distinguish them from the diamagnetic His backbone amides and that are consistent with these nuclei being H-bonded to the iron−sulfur center.

If the basic ISP structure is conserved in reduced T4MOC (see Figure 9 and discussion below), one amide nitrogen of the histidine ligands to the ferrous site will donate an H-bond to the S^{γ} of one of the cysteine ligands, the other His amide nitrogen will donate an H-bond to one of the μ-sulfide bridges, and the amide nitrogens of the two cysteine ligands to the ferric site will not be H-bonded to the cluster. However, despite the likely difference in localized electronic environment given by this H-bonding pattern, all hyperfine-shifted nitrogen nuclei observed in reduced T4MOC exhibit Curie temperature dependence. A similar result has been observed in both ^{13}C and ^{15}N studies of reduced *Anabaena* ferredoxin (*25*).

Although our ^{15}N NMR studies of [$^{15}N^{\delta 1}$]His T4MOC revealed no hyperfine-shifted signals in either oxidation state,

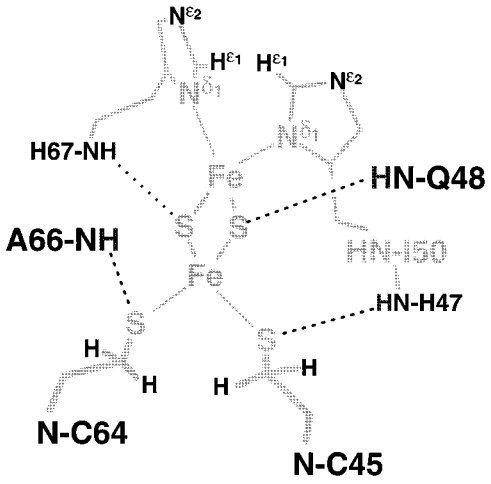

FIGURE 9: Model for the Rieske cluster in T4MOC based on the crystal structure of the bc_1 ISP domain (*10*), amino acid sequence alignments, and the NMR measurements reported here. All nuclei indicated in bold face were identified by selective labeling. No hyperfine shifted ^{15}N resonances were observed from H47 $N^{\delta 1}$, I50 N, or H67 $N^{\delta 1}$. The proposed H-bonds from H67 N and Q48 N to the bridging sulfides, H47 N to C45 S^{γ}, and A66 N to C64 S^{γ} are consistent with the hyperfine-shifted ^{15}N NMR signals reported in Table 2.

two hyperfine-shifted ^{15}N resonances were observed from [$^{15}N^{\delta 1,\epsilon 2}$]His T4MOC and were thus assigned to the $N^{\epsilon 2}$ atoms of cluster ligands H47 and H67. Since $N^{\delta 1}$ of His is bonded to an iron site in all other structurally characterized Rieske proteins, as revealed by ENDOR (*8*), ESEEM, (*7*, *9*), and X-ray crystallography (*10*−*12*), our inability to detect a ^{15}N NMR resonance from [$^{15}N^{\delta 1}$]His T4MOC must arise from the extremely short relaxation time of ^{15}N directly bonded to high spin ferrous and/or an unusually large hyperfine shift.

Comparison to Other Rieske Proteins. The similar UV−vis, EPR, and Mössbauer properties determined for the Rieske proteins are consistent with the strong antiferromagnetic coupling of the bis-μ-sulfido core and the asymmetric ligation of the iron atoms. However, other techniques such as electrochemistry, ESEEM, and ENDOR have revealed subtle differences among the Rieske proteins isolated from a wide variety of organisms and catalytic systems (*7*−*9*, *45*, *46*). The clarification of how these differences arise from the surrounding protein environment (*47*, *48*) and then contribute to the diversity of function is a critical topic in metalloprotein biochemistry (*49*).

Figure 1 shows an alignment of the amino acid sequences containing the metal-binding motifs of T4MOC, NDO, and the ISP domains from chloroplasts and bovine mitochondrion. In this sequence of 40 amino acids, only the four ligands to the Rieske center (C45, H47, C64, and H67 in T4MOC) and one Pro residue are conserved. The proline residue, P81 in T4MOC, corresponds to P175 in ISP. In the ISP domain, the sequence −Gly-Pro175-Ala-Pro− forms one of the three β-strand loops that define the metal-binding site. This sequence is exactly conserved in all ISP domains, and single mutations of any of the four residues within this loop have been shown to destabilize the cluster (*1*, *50*−*52*). In T4MOC (P81) and NDO (P118), proline residues are found at the same spacing after the metal-binding motif as P175 in ISP; however, none of the other four adjacent residues is conserved between T4MOC, NDO, and the ISP domain. Furthermore, the ISP residues found to be conserved with

the *Desulfovibrio vulgaris* rubredoxin metal-binding fold (G143, P159, and G162) are not conserved in either T4MOC (E49, R65, and L68, respectively) or NDO. It is also notable that the cysteine residues forming the disulfide bond in the ISP domain are not conserved in T4MOC, but are substituted by I50 and A66 in the homologous positions of T4MOC (K86 and Y103 occupy the homologous positions in NDO). In T4MOC, these substitutions provide a side-chain volume (~191 Å) similar to that of cystine (~172 Å), but cannot provide the redox-dependent structural stability found in the ISP fragment. Furthermore, of I50 and A66, only A66 is hydrogen bonded to the cluster of T4MOC as judged by ^{15}N NMR, providing an example of how structural variations in T4MOC relative to ISP can influence electronic properties of the active site.

Figure 1 also shows residues identified by crystallography to provide H-bonds to the inorganic sulfides and the cysteine S^{γ} atoms of the ISP cluster. Of these seven H-bonds, five are provided by peptidyl N−H groups [indicated by an asterisk (*) in Figure 1]. The present ^{15}N NMR studies have shown that four of these five peptidyl N−H bonds are present in T4MOC and are likely provided by H47, Q48, A66, and H67. Due to the unusual exchange properties, we propose that the −12.3 ppm ^{1}H resonance of reduced T4MOC may arise from one of the H-atom(s) in these peptidyl N−H bonds to the Rieske cluster. The remaining two H-bonds to the ISP cluster, which mutagenesis studies have revealed are absolutely essential for cluster stability (*1*), are provided by $H-O^{\gamma}$ of a serine and $H-O^{\eta}$ of a tyrosine [S163 and Y165, respectively, indicated by a solid circle (●) in Figure 1]. Neither of these two H−O bonding residues are conserved in T4MOC, which contains W69 and F71, respectively. In the NDO crystal structure, the position of serine is occupied by W106, which covers one side of the Rieske center (*13*). This similarity suggests that the T4MOC Rieske cluster may likewise be partially capped by interaction with W69.

Correlated Model for the T4MOC Cluster Core. Our current model for the T4MOC cluster core is shown in Figure 9. This model incorporates the aspects of the T4MOC amino acid sequence and the NMR studies described here that are consistent with the H-bonding pattern established by the available Rieske protein crystal structures (Figure 1). The T4MOC residues C45, H47, C64, and H67 correspond to the Rieske protein metal-binding motif. The ^{1}H NMR measurements of Figure 2 and the ^{15}N NMR measurements of Figures 6 and 7 indicate that C45 and C64 are ligands to the localized ferric site of the reduced Rieske cluster. The ^{15}N NMR measurements also indicate that $N^{\delta 1}$ of both H47 and H67 are ligands to the localized ferrous site in the reduced protein, which is consistent with crystallographic and spectroscopic studies of all other Rieske proteins. As in the ISP domain, the peptidyl N−H groups of T4MOC residues H47 and H67 likely form H-bonds to the cluster. This conclusion is consistent with the observation of two inequivalent, hyperfine-shifted His ^{15}N resonances in both the oxidized and reduced states (Figure 7). Since H47 and H67 are comparable to residues in the ISP domain that are H-bonded to a Cys S^{γ} and a μ-sulfido bridge position, respectively, the differences in unpaired electron density at these two positions may indeed be the origin of the differences in ^{15}N chemical shifts recorded here for T4MOC. Peptidyl N−H bonds are also provided by Q48 and A66, with Q48 providing an H-bond (possibly to a μ-sulfido position) that increases dramatically in strength upon reduction.

ACKNOWLEDGMENT

We thank Dr. C. J. Unkefer (Los Alamos Stable Isotope Resource) for providing the [$^{15}N^{\delta 1,\epsilon 2}$]-D,L-His and Dr. T. A. Link for helpful comments on enzyme nomenclature.

REFERENCES

1. Trumpower, B. L., and Gennis, R. B. (1994) *Annu. Rev. Biochem. 63*, 675−716.
2. Cammack, R. (1992) *Adv. Inorg. Chem. 38*, 281−322.
3. Mason, J. R., and Cammack, R. (1992) *Annu. Rev. Microbiol. 46*, 277−305.
4. Fee, J. A., Findling, K. L., Yoshida, T., Hille, R., Tarr, G. E., Hearshen, D. O., Dunham, W. R., Day, E. P., Kent, T. A., and Münck, E. (1984) *J. Biol. Chem. 259*, 124−133.
5. Cline, J. F., Hoffman, B. M., Mims, W. B., LaHaie, E., Ballou, D. P., and Fee, J. A. (1985) *J. Biol. Chem. 260*, 3251−3254.
6. Gurbiel, R. J., Batie, C. J., Sivaraja, M., True, A. E., Fee, J. A., Hoffman, B. M., and Ballou, D. P. (1989) *Biochemistry 28*, 4861−4871.
7. Shergill, J. K., Joannou, C. L., Mason, J. R., and Cammack, R. (1995) *Biochemistry 34*, 16533−16542.
8. Gurbiel, R. J., Doan, P. E., Gassner, G. T., Macke, T. J., Case, D. T., Ohnishi, T., Fee, J. A., Ballou, D. P., and Hoffman, B. M. (1996) *Biochemistry 35*, 7834−7845.
9. Dikanov, S. A., Xun, L., Karpiel, A. B., Tyryshkin, A. M., and Bowman, M. K. (1996) *J. Am. Chem. Soc. 118*, 8408−8416.
10. Iwata, S., Saynovits, M., Link, T. A., and Michel, H. (1996) *Structure 4*, 567−579.
11. Link, T. A., and Iwata, S. (1996) *Biochim. Biophys. Acta 1275*, 54−60.
12. Carrell, C. J., Zhang, H., Cramer, W. A., and Smith, J. L. (1997) *Structure 5*, 1613−1625.
13. Kauppi, B., Lee, K., Carredano, E., Parales, R. E., Gibson, D. T., Eklund, H., and Ramaswamy, S. (1998) *Structure 6*, 571−586.
14. Pikus, J. D., Studts, J. M., Achim, C., Kauffmann, K. E., Münck, E., Steffan, R. J., McClay, K., and Fox, B. G. (1996) *Biochemistry 35*, 9106−9119.
15. Whited, G. M., and Gibson, D. T. (1991) *J. Bacteriol. 173*, 3010−3016.
16. Denke, E., Merbitz-Zahradnik, T., Hatzfeld, O. M., Snyder, C. H., Link, T. A., and Trumpower, B. L. (1998) *J. Biol. Chem. 273*, 9085−9093.
17. Markley, J. L., Xia, B., Chae, Y. K., Cheng, H., Westler, W. M., Pikus, J. D., and Fox, B. G. (1996) in *Protein Structure Function Relationships*, (Zaidi, Z., and Smith, D., Eds.) pp 135−146, Plenum Press, London.
18. Holz, R. C., Small, F. J., and Ensign, S. A. (1997) *Biochemistry 36*, 14690−14696.
19. Yen, K.-M., Karl, M. R., Blatt, L. M., Simon, M. J., Winter, R. B., Fausset, P. R., Lu, H. S., Harcourt, A. A., and Chen, K. K. (1991) *J. Bacteriol. 173*, 5315−5327.
20. Hoffman, B. J., Broadwater, J. A., Johnson, P., Harper, J., Fox, B. G., and Kenealy, W. R. (1995) *Protein Expression Purif. 6*, 646−654.
21. Sambrook, J., Fritsch, E. F., and Maniatis, T. (1989) in *Molecular Cloning, A Laboratory Manual*, Cold Spring Harbor Laboratory Press, Plainview, NY.
22. Markley, J. L., Bax, A., Arata, Y., Hilbers, C. W., Kaptein, R., Sykes, B. D., Wright, P. E., and Wüthrich, K. (1998) *Pure Appl. Chem. 70*, 117−142.
23. Markley, J. L. (1975) *Acc. Chem. Res. 8*, 70−80.
24. Xia, B., Cheng, H., Skjedal, L., Coghlan, V. M., Vickery, L. M., and Markley, J. L. (1995) *Biochemistry 34*, 180−187.
25. Cheng, H., Westler, W. M., Xia, B., Oh, B.-H., and Markley, J. L. (1995) *Arch. Biochem. Biophys. 316*, 619−634.

26. Bax, A., Griffey, R. H., and Hawkins, B. L. (1983) *J. Magn. Reson. 55*, 301.
27. Sklenar, V., and Bax., A. (1987) *J. Magn. Reson. 74*, 469−497.
28. Sands, R. H., and Dunham, W. R. (1975) *Q. Rev. Biophys. 7*, 443−504.
29. Poe, M., Phillips, W. D., Glickson, J. D., McDonald, C. C., and Pietro, A. S. (1971) *Proc. Natl. Acad. Sci. U.S.A. 68*, 68−71.
30. Skjeldahl, L., Westler, W. M., and Markley, J. L. (1990) *Arch. Biochem. Biophys. 278*, 482−485.
31. Cheng, H., Xia, B., Reed, G. H., and Markley, J. L. (1994) *Biochemistry 33*, 3155−3164.
32. Xia, B., Cheng, H., Bandarian, V., Reed, G. H., and Markley, J. L. (1995) *Biochemistry 35*, 9488−9495.
33. Cheng, H., and Markley, J. L. (1995) *Annu. Rev. Biophys. Biomol. Struct. 24*, 209−237.
34. Skjeldahl, L., Markley, J. L., Coghlan, V. M., and Vickery, L. E. (1991) *Biochemistry 30*, 9078−9083.
35. Cook, P. F., Tai, C. H., Hwang, C. C., Woehl, E. U., Dunn, M. F., and Schnackerz, K. D. (1996) *J. Biol. Chem. 271*, 25842−92584.
36. Kredich, N. M. (1971) *J. Biol. Chem. 246*, 3474−3484.
37. Xia, B., Westler, W. M., Cheng, H., Meyer, J., Moulis, J.-M., and Markley, J. L. (1995) *J. Am. Chem. Soc. 117*, 5347−5350.
38. Hurley, J. K., Caffrey, M. S., Markley, J. L., Cheng, H., Xia, B., Chae, Y. K., Holden, H. M., and Tollin, G. (1995) *Protein Sci. 4*, 58−64.
39. Creighton, T. E. (1994) *Proteins: Structure and Molecular Properties*, pp 13−14, W. H. Freeman, New York.
40. Fox, B. G. (1997) in *Comprehensive Biological Catalysis* (Sinnott, M., Ed.) pp 261−348, Academic Press, London.
41. Orme-Johnson, N. R., Mims, W. B., Orme-Johnson, W. H., Bartsch, R. G., Cusanovich, M. A., and Peisach, J. (1983) *Biochim. Biophys. Acta 748*, 68−72.
42. Pochapsky, T. C., Ratnaswamy, G., and Patera, A. (1994) *Biochemistry 33*, 6433−6441.
43. Lyons, T. A., Ratnaswamy, G., and Pochapsky, T. C. (1996) *Protein Sci. 5*, 627−639.
44. Dugad, L. B., La Mar, G. N., Banci, L., and Bertini, I. (1990) *Biochemistry 298*, 2263−2271.
45. Link, T. A., Hagen, W. R., Pierik, A. J., Assmann, C., and von Jagow, G. (1992) *Eur. J. Biochem. 208*, 685−691.
46. Link, T. A., Hatzfield, O. M., Unalkat, P., Shergill, J. K., Cammack, R., and Mason, J. R. (1996) *Biochemistry 35*, 7546−7552.
47. Backes, G., Mino, Y., Loehr, T. M., Meyer, T. M., Cusanovich, M. A., Sweeny, W. V., Adman, E. T., and Sanders-Loehr, J. (1991) *J. Am. Chem. Soc. 113*, 2055−2064.
48. Stephens, P. J., Jollie, D. R., and Warshel, A. (1996) *Chem. Rev. 96*, 2491−2513.
49. Beinert, H., Holm, R. C., and Münck, E. (1997) *Science 277*, 653−659.
50. Moulis, J.-M., Davasse, V., Golinelli, M.-P., Meyer, J., and Quinkal, I. (1996) *J. Biol. Inorg. Chem. 1*, 2−14.
51. Davidson, E., Ohnishi, T., Atta-Asafo, A., and Daldal, F. (1992) *Biochemistry 31*, 3342−3351.
52. Liebl, U., Sled, V., Brasseur, G., Ohnishi, T., and Daldal, F. (1997) *Biochemistry 36*, 11675−11684.

BI981851A